Polaron theory of positron annihilation in xenon

Jiqiang Chen and Bruce N. Miller
Department of Physics, Texas Christian University, Fort Worth, Texas 76129
(Received 21 June 1993)

Experimental measurements of the annihilation rate of a positron in fluid xenon show that it exhibits an anomalously nonlinear dependence on the fluid density. Recent path-integral Monte Carlo simulations of the system suggest that the nonlinearity results from the formation of xenon clusters which surround the positron at moderate densities. In this paper we investigate the ability of the analytic reference-interaction-site-model–(RISM) polaron theory to replicate these results, and provide richer information concerning the e^+-xenon system over a wider range of circumstances. Two distinct closures of the RISM equation are considered, as well as the effects of altering the attractive part of the potential. The main results are that, when coupled with the hypernetted-chain closure, the theory qualitatively reproduces the main features of the experiments and Monte Carlo simulations, but underestimates the cluster density and confinement of the localized positron.

PACS number(s): 05.30.−d, 71.60.+z, 78.70.Bj, 36.10.Dr

I. INTRODUCTION

Positron annihilation has been an interesting field since the early 1960s when it was realized that the annihilation photons carried useful information about the structure of the material in which the positron annihilated. Because of the complexity of the quantum states of the positron, many aspects of positron annihilation in fluids have not been understood well. Recently, Miller and co-workers carried out path-integral Monte Carlo (PIMC) calculations of positron and postronium annihilation in xenon at different temperatures and fluid densities [1,2]. Along with the earlier PIMC studies of an excess electron in helium and xenon by Coker, Berne, and Thirumalai [3], these simulations offer some insights for a better understanding of the behavior of these light particles in simple fluids. In this paper we present an adaptation of the reference-interaction-site-model–polaron theory to the problem of positron localization in xenon over a variety of fluid densities ρ at a given temperature ($T=340$ K) and compare its predictions with its PIMC counterpart.

Reference-interaction-site-model (RISM) theory was originally introduced by Chandler to study the structure of molecular fluids [4]. Since the introduction of the path integral by Feynman [5], physicists have known how to represent a quantum particle (QP) by a classical ring polymer with p ($p\rightarrow\infty$) classical interacting harmonic oscillators (classical isomorphism). Chandler and coworkers recognized that, in this form, an excess quantum particle that has thermalized in a classical fluid could be described within the context of classical fluid theory. By joining Feynman's polaron approximation [5(b)] with the RISM theory, they developed an analytical representation of the particle-fluid system which they used to study the localization of a hard-spherical quantum particle in a simple fluid [6]. As in the case of a classical fluid, for the purposes of computation RISM theory requires a closure assumption. In their original studies Chandler *et al.* imposed the PY-like (Percus-Yevick) closure [7] for the correlation between the quantum particle and a fluid atom. Later the approach was modified by Malescio and Parrinello in their study of an electron solvated in a molten salt [8]. Because here the quantum particle interacts with postassium and chlorine ions through long-range Coulomb potentials intead of a hard sphere, they selected a hypernetted-chain- (HNC-) like closure [9]. More recently, a closure was proposed and applied to the problem of the hydrated electron [10]. By comparing the predictions of RISM-polaron theory with their computer-simulation counterparts, one finds that the theory offers a good foundation for the understanding of quantum particle localization in fluids.

There are some other theories available for modeling quantum particle localization in fluids. Notable among these is density-functional theory (DFT), which provides a fairly successful description of some aspects of the localization phenomena [11]. DFT is essentially a mean-field theory that characterizes the system by a single, optimal wave function representing the QP, and a smooth, local, nonuniform fluid density representing its environment. Although fluctuations play an important role in the localization process, DFT does not take them into account, and consequently fails to give a correct picture of localization. For example, in DFT the existence of localized solutions abruptly turns on and off at specific values of the fluid density, whereas experimental data show a continuous transition from extended to localized behavior. Although one mean-field approximation is involved in RISM-polaron theory [6], it does take some fluctuations into consideration and therefore the picture of localization in terms of the RISM-polaron theory is quite different from that of density-functional theory.

The only numerically exact way to treat the present system is via computer simulation. Of the two major approaches, PIMC and quantum molecular dynamics, the former is more successful for equilibrium properties because it does not require truncation of the state space or

"regularization" of the interaction potential. But PIMC is very CPU intensive and can only test a few points, so it is difficult to obtain a good picture of the predictions over the complete range of density and temperature. Mean-field theory only gives nontrivial solutions over a finite range of temperature and density, and certainly fails in the transition region from localized to extended states, where fluctuations dominate. Currently the RISM-polaron theory is the only existing analytical theory that covers the complete range. Therefore it is desirable to test the RISM-polaron theory against known PIMC results. This work serves two purposes: to display the general picture of positron localization in xenon, and to show the usefulness of the RISM-polaron theory for this sort of problem.

The paper is organized as follows: The RISM-polaron theory for a positron in xenon is presented in Sec. II; the computational method is described and the numerical results are presented in Sec. III; the results are interpreted and conclusions are summarized in Sec. IV.

II. RISM-POLARON THEORY OF A POSITRON IN XENON

We consider a single positron dissolved in fluid xenon in the adiabatic approximation in which the positron is treated quantum-mechanically and xenon atoms classically. From a standard imaginary-time path-integral formulation [5(a)], this system is identical to a classical ring polymer dissolved in the solvent and can be described by the RISM-polaron theory. The basic setup for deriving the RISM-polaron approximation from the discrete ring-polymer model is described by Chandler and co-workers in Ref. [6], and we proceed from there. The RISM equation

$$\rho h(r)=\int d\mathbf{r}'\int d\mathbf{r}''\omega(|\mathbf{r}-\mathbf{r}'|)c(|\mathbf{r}'-\mathbf{r}''|)\chi(|\mathbf{r}''|) \tag{1}$$

with a closure

$$c(r)=F[h(r)] \tag{2}$$

provides the connection between the positron-solvent direct-correlation function $c(r)$ and the positron-fluid pair-correlation function $h(r)$. In Eq. (1), $\chi(r)$ is the solvent density-density correlation

$$\chi(|\mathbf{r}-\mathbf{r}'|)=\langle\delta\rho(\mathbf{r})\delta\rho(\mathbf{r}')\rangle\ , \tag{3}$$

which represents the structural influence of the fluid on the state of the light particle and $\omega(r)$ is the zero-frequency component of the polymer probability density function $\omega(r,\tau)$:

$$\omega(r)=(\beta\hbar)^{-1}\int_0^{\beta\hbar}d\tau\,\omega(r,\tau)\ , \tag{4}$$

where

$$\omega(\mathbf{r},\mathbf{r}';i,j)\equiv\omega(|\mathbf{r}-\mathbf{r}'|;i-j)\rightarrow\omega(|\mathbf{r}-\mathbf{r}'|;\tau-\tau')\quad(p\rightarrow\infty) \tag{5}$$

represents the polymer probability density for finding polymer sites i and j near $\mathbf{r}$ and $\mathbf{r}'$, respectively, in the limit of a continuous chain.

In (2), $F[h]$ denotes a functional of $h(r)$ and must be approximated in practice. One closure being used widely in simple atomic fluids is the so-called HNC closure,

$$c(r)=\exp\{-\beta V(r)+[h(r)-c(r)]\}-[h(r)-c(r)]-1\ , \tag{6}$$

which is a good approximation for fluids with a long-range interatomic potential. We accept (6) as a closure to the RISM equation (1) applied to our system, where $V(r)$ is taken as the positron-solvent interaction.

The interaction between a positron and a xenon atom is not known exactly. For their PIMC calculations [1], Worrell and Miller used the following analytical potential to describe the interaction:

$$V(r)=\frac{Z}{r}[a\exp(-c_1r)+(1-a)\exp(-c_2r)]-\alpha\frac{1-\exp[-(r/r_0)]^6}{2r^4}\ , \tag{7}$$

which is based on Schrader's work [12] on constructing the potential from the Hartree-Fock potential of the isolated xenon atom and a contribution produced by the large atomic polarizability. The static polarization and the atomic number of the xenon atom are, respectively, $\alpha=26.92$ a.u., and $z=54$. The values for the other parameters in (7) are $a=0.336$ and, in atomic units, $c_1=1.360$, $c_2=6.280$, and $r_0=2.15$.

The second term of the potential is due to the polarization of the xenon atom and is the dominant part at large distance. Since the xenon atom is easily polarized, the long-range potential must play a crucial rule and be treated carefully. In particular, we expect that $c(r)$, the direct correlation function of the positron with the fluid atoms, takes the form

$$c(r)=-\beta\frac{\alpha\{1-\exp[-(r/r_0)^6]\}}{2r^4}\rightarrow-\beta\frac{\alpha}{2r^4} \tag{8}$$

at large distance.

Following Malescio and Parrinello [8], we write

$$c(r)=c_s(r)+c_l(r)\ , \tag{9}$$

where $c_s(r)$ and $c_l(r)$ are the short- and long-range parts of the direct correlation function $c(r)$, respectively. In this work we simply take (8) as $c_l(r)$ for all r. This choice will be discussed further below. Thus, if we know $c_s(r)$, we will be able to obtain all the information about the positron in the fluid.

To obtain $c_s(r)$, we consider the decomposition of $c(r)$ in (9). The RISM equation (1) can be written in the form

$$\begin{aligned}\rho h(r)&=\int d\mathbf{r}'d\mathbf{r}''\omega(|\mathbf{r}-\mathbf{r}'|)c_s(|\mathbf{r}'-\mathbf{r}''|)\chi(\mathbf{r}'')\\&\quad+\int d\mathbf{r}'\int d\mathbf{r}''\omega(|\mathbf{r}-\mathbf{r}'|)c_l(|\mathbf{r}'-\mathbf{r}''|)\chi(\mathbf{r}'')\\&\equiv\langle c_s\rangle+\langle c_l\rangle\ .\end{aligned} \tag{10}$$

Denoting the short-range part (the first term) of the po-

tential (7) as $V_s(r)$ and noting that $c(r)=c_s(r)+c_l(r)$ and $c_l(r)=-\beta V_l(r)$, the closure for $c_s(r)$ and $h(r)$ is given in the form

$$\begin{aligned} c_s(r)&=\exp\{-\beta V_s(r)+[h(r)-c_s(r)]\} \\ &\quad -[h(r)-c_s(r)]-1 \\ &\equiv\exp[-\beta V_s(r)+\langle c_l\rangle+\theta(r)] \\ &\quad -\langle c_l\rangle-\theta(r)-1 , \end{aligned} \tag{11}$$

where $\theta(r)=h(r)-c_s(r)-\langle c_l\rangle$, which is just the closure used by Malescio and Parrinello for their solvated electron in a molten salt [8]. It is interesting to note that $c_l(r)$ and $V_l(r)$ are not explicitly involved in (11). For given $\omega(r,\tau)$ and $\chi(r)$, a solution for $h(r)$ and $c_s(r)$ can be found from Eqs. (10) and (11).

The remainder of the theory concerns the polymer probability density function $\omega(r,\tau)$. In the polaron approximation, it can be determined self-consistently from the following equations:

$$\bar{\omega}(k,\tau)=\exp\left[-k^2\sum_{n\,(\neq 0)}\frac{1-\cos\Omega_n\tau}{\beta m\Omega_n^2+\gamma_n}\right] , \tag{12}$$

$$\gamma_n=(6\pi^2\beta\hbar)^{-1}\int_0^\infty dk\,k^4\bar{c}^{\,2}(k)\bar{\chi}(k) \times\int_0^{\beta\hbar}d\tau(1-\cos\Omega_n\tau)\bar{\omega}(k,\tau) \tag{13}$$

for given $\bar{\chi}(k)$ and $\bar{c}(k)=\bar{c}_s(k)+\bar{c}_l(k)$, where $\bar{\omega}(k,\tau)$, $\bar{c}(k)$, and $\bar{\chi}(k)$ are the Fourier transform of $\omega(r,\tau)$, $c(r)$, and $\chi(r)$, respectively, and $\Omega_n=2n\pi/\beta\hbar$. To speed up the summation in (12), we follow Fan and Miller [13] to rewrite it in the form

$$\begin{aligned} Q(\tau)&=\sum_{n\,(\neq 0)}\frac{1-\cos\Omega_n\tau}{\beta m\Omega_n^2+\gamma_n} \\ &=\sum_{n\,(\neq 0)}\frac{1-\cos\Omega_n\tau}{\beta m\Omega_n^2} \\ &\quad -\sum_{n(\neq 0)}\frac{1-\cos\Omega_n\tau}{\beta m\Omega_n^2(\beta m\Omega_n^2+\gamma_n)} \\ &=Q_1(\tau)-Q_2(\tau) . \end{aligned} \tag{14}$$

Q_1 corresponds to a noninteracting light particle and can be evaluated exactly,

$$Q_1(\tau)=(\lambda^2/2)\tau(\beta\hbar-\tau)/(\beta\hbar)^2 , \tag{15}$$

where $\lambda^2=\beta\hbar^2/m$ is the thermal wavelength of the positron, m is its mass, and Q_2 is the correction to Q_1. We will see that including just a few terms in Q_2 can give quite satisfactory results.

III. METHOD AND RESULTS OF CALCULATIONS

Equations (10)–(13) form a self-consistent system. We start with an assumed set of $(\gamma_1,\gamma_2,\ldots,\gamma_n)$ and obtain the initial $\bar{\omega}(k,\tau)$ from Eq. (12). Then we take $\theta(r)$ as the iteration variable to achieve the convergent solutions for $h(r)$ and $c(r)$ from Eqs. (10) and (11) for the given γ's and $\bar{\omega}(k,\tau)$. From Eq. (13) we obtain a new set of γ's and repeat the above procedure until the γ's achieve the required accuracy.

The iterative solution of Eqs. (10) and (11) is carried out via fast Fourier transformation (FFT) techniques on a grid of $N=2^{11}$ points equally spaced with $\Delta r=0.037\,03$ Å. This also allows the use of the RISM equation (10) in k space.

$$\begin{aligned} \rho\bar{h}(k)&=\bar{\omega}(k)\bar{c}(k)\bar{\chi}(k) \\ &=\bar{\omega}(k)\bar{c}_s(k)\bar{\chi}(k)+\bar{\omega}(k)\bar{c}_l(k)\bar{\chi}(k) \end{aligned} \tag{16}$$

which is simpler in form and easier to use. We require the error in $h(r)$ at $r=0$ to be less than 0.001 [$h(0)$ should equal -1.0 as the potential (7) is infinite at $r=0$] and the quantity

$$\Delta\theta=\left|\sum_{i=1}^{N}[\theta^{m+1}(r_i)-\theta^m(r_i)]^2/N\right|^{1/2} \tag{17}$$

to be less than 0.001. To accelerate convergence, the Ng method is used in which the mth iteration input is obtained as a suitable linear combination of the preceding three iterations [14]. Furthermore, for $\rho^*>0.3$, we do the calculation from high to low fluid density, so that we can use the output $\theta(r)$ from the next-higher density as input to the lower density because we have found that it was more difficult to achieve convergence proceeding in the other direction. For densities $\rho^*<0.3$, we proceed in the opposite direction. In spite of all of these efforts, between 10^3 and 10^4 iterations are still required to achieve the stated accuracy in $h(r)$ for a given set of γ's. The τ integrals in Eqs. (4) and (13) are carried out by a self-adjusting mesh integration program so that an accuracy of 10^{-5} is guaranteed regardless of the shape of the integrands [13]. As for the number of γ values selected, we found that there was no significant difference in the final results when we included the first ten values ($n=10$) or the first 30 values ($n=30$). Fewer than ten iterations of the entire process yielded at least three-digit accuracy for the γ's.

To accomplish the present study, we need χ as input. RISM-polaron theory can only be as good as χ. The best possible χ can, of course, be obtained from Monte Carlo or molecular-dynamics calculations, but this defeats the purpose of constructing a theoretical model. The best candidate seems to be given by the solutions of the reference-hypernetted-chain (RHNC) equation of simple classical fluids [15]. Lado, Foiles, and Ashcroft [15] used the Rosenfeld-Ashcroft procedure to model the bridge function in the RHNC integral equation with its hard-sphere values, and choose the sphere diameter so that the free energy of the system is minimized. The RHNC equation for simple fluids has also been tested recently by an alternative computational procedure [16]. The results given in [15,16] show that the difference between the solutions of RHNC and the simulation studies are comparable to the uncertainties in the simulation data. For the present calculation, we use the procedure of Lado, Foiles, and Ashcroft to generate the structure factor $S(k)$ of the RHNC solution for xenon with a Lennard-Jones potential ($\sigma=4.0551$ Å and $\epsilon=229$ K) at $T=340$ K and

various densities to obtain $\bar{\chi}(k)=\rho S(k)$, the Fourier transformation of $\chi(r)$.

Figure 1 shows the structure factor $S(k)$ of xenon at three representative densities. We see that when the fluid density approaches its critical value (the critical density $\rho^*=\rho\sigma^3\approx 0.35$ for the Lennard-Jones fluid [1]), $S(k\rightarrow 0)$ increases. This is a basic feature of real fluids and implies that the isothermal compressibility becomes large at the critical point, while a hard-sphere fluid lacks such behavior. The behavior of $S(k)$ at small k is important in RISM-polaron theory because $\bar{\omega}(k,\tau)$ is a Gaussian function in k and therefore values of $S(k)$ at small k are sampled preferentially and contribute more to $\bar{h}(k)$ through Eq. (16). This supports the experimental observation that localization is enhanced in the critical region where the compressibility is large, causing the fluid to respond more strongly to the presence of the QP. Since we are calculating at $T=340$ K rather than at the critical temperature $T_c=289$ K, we have found that $S(k=0)$ achieves its maximum value at around $\rho^*=0.25$.

A quantitative measure of the size of the polymer (or continuous path in the limit $p\rightarrow\infty$) is $R(\beta\hbar/2)$, the root-mean-square separation between two points, or beads, located half-way around the polymer. It is easily obtained from the second moment of $\omega(\mathbf{r},\tau=\beta\hbar/2)$, which yields $R(\beta\hbar/2)=[6Q(\beta\hbar/2)]^{1/2}$. For a free particle, $R_{\text{free}}(\beta\hbar/2)=3^{1/2}\lambda/2$. Therefore

$$P=\frac{R(\beta\hbar/2)}{R_{\text{free}}(\beta\hbar/2)}=\frac{2R(\beta\hbar/2)}{3^{1/2}\lambda} \tag{18}$$

provides a measure of the relative localization of the positron. In Fig. 2 the relative size P is plotted as a function of fluid density ρ^* at $T=340$ K both for the RISM-polaron calculation and for the corresponding PIMC results. From the figure we see that the positron with potential (7) is delocalized at low and high densities ($P\approx 1$) but becomes compressed at some intermediate values. The most compressed state predicted by the RISM-polaron theory is located at around $\rho^*=0.25$, which coincides with the density where $S(k=0)$ gets its maximum. This state seems to occur at a higher density than the most compressed state given by PIMC at the same temperature, which appears to be located just below

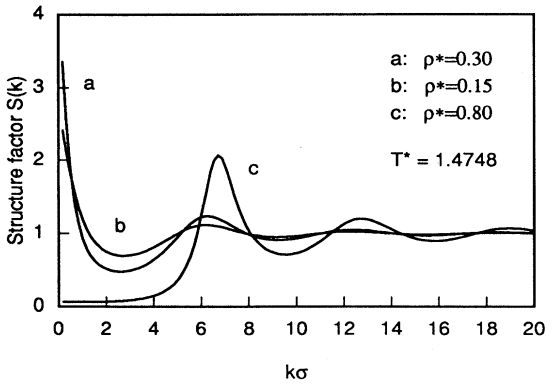

FIG. 1. Structure factor $S(k)$ for xenon resulting from the RHNC solutions of Lado, Foiles, and Ashcroft [15].

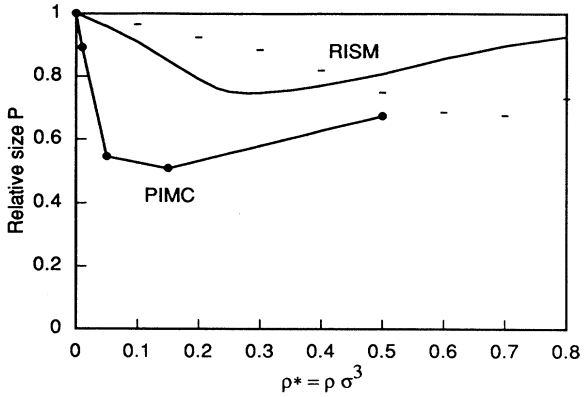

FIG. 2. The dependence of P on xenon density at temperature $T=340$ K from PIMC and RISM-polaron calculations. (The RISM-polaron results using only the repulsive screened nuclear part of the potential [the first term in (7)] is also plotted (dashed line)).

$\rho^*=0.2$. Since we only have the PIMC results at a few points, we cannot be more precise. However, the overall picture is clear. The qualitative picture presented by the RISM-polaron theory agrees with the PIMC simulations, but the positron polymer is less compressed in the RISM-polaron theory.

We now examine $g(r)=1+h(r)$, the positron-solvent radial distribution function, which provides a measure of the influence of the QP on its local environment. Worrell and Miller carried out PIMC simulations for $\rho^*=0.01$, 0.05, 0.15, and 0.5 [1]. The general behavior they found is that $g(r)=0$ at small r, then rises rapidly to a strong peak at the location where the positron potential (7) assumes its minimum value, and decays rapidly afterwards. The strong peak indicates the formation of a xenon atom cluster around the positron. This beahvior is reproduced by the RISM-polaron theory, and we illustrate $g(r)$ for some representative densities in Fig. 3 (upper graph).

It is worth pointing out that RISM-polaron theory predicts that, at higher densities, where PIMC simulations have not been carried out, $g(r)$ undergoes an oscillating decay beyond the primary peak. Oscillations did not occur in the PIMC simulations at lower density. This needs to be examined in more detail by PIMC but, nonetheless, it seems to be the real behavior. Both the PIMC and RISM-polaron calculations for an electron in xenon exhibit a similar oscillation [3,17].

Our calculations do reveal some disagreements between RISM-polaron and PIMC for low density. To show this, in Fig. 3 (lower graph) we also plot the value of the first peak in $g(r)$ versus fluid density. By comparing this with Fig. 2 we can see that, in the RISM-polaron picture, there is a direct correspondence between the degree of polymer compression and the height of the peak of $g(r)$. The more compressed the positron polymer, the higher the peak. This correspondence does not occur in the PIMC simulations, in which the highest peak is located at a lower density than the most compressed state. Furthermore, the peak given by PIMC is generally higher than that of RISM-polaron theory. In addition, we no-

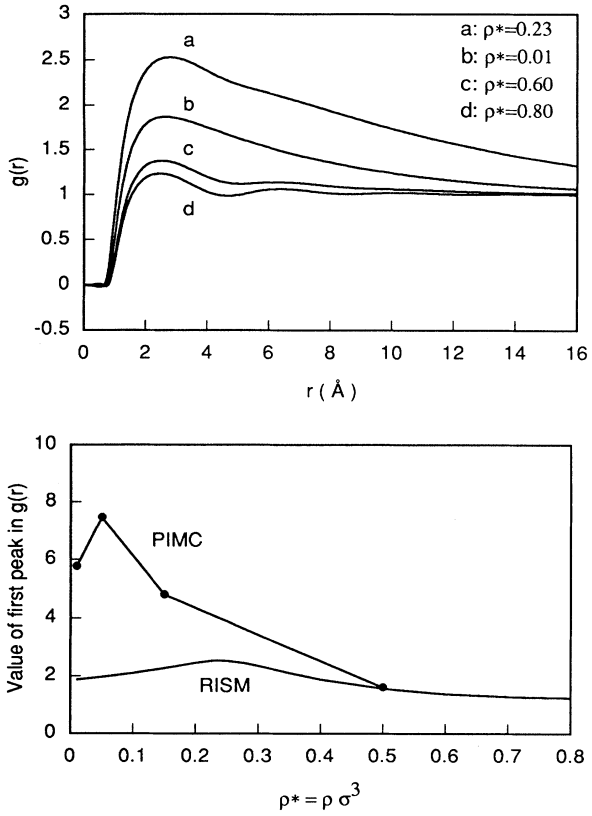

FIG. 3. Upper graph: positron-xenon radial distribution function $g(r)$ for some representative fluid densities at $T=340$ K from RISM-polaron calculations; lower graph: the dependence of the value (height) of the first peak of $g(r)$ on fluid density at $T=340$ K from both PIMC and RISM-polaron calculations.

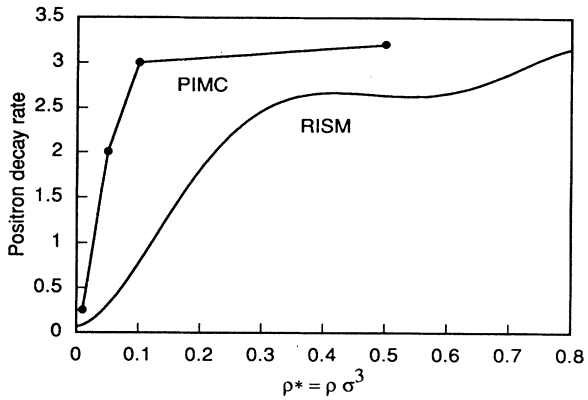

FIG. 4. Positron decay rate vs fluid density at $T=340$ K from PIMC and RISM-polaron calculations.

tice that the radial distribution function plotted in Fig. 3 decays much more slowly than that obtained from PIMC [1]. In other words, the first peak is broader in the RISM-polaron theory. This might be considered as compensation for its weaker first peak, so that the size of xenon clusters predicted by each model may be approximately equal. To determine this requires a correlation function, or local density, in which the center of mass of the polymer is fixed at the origin. While this is readily available in PIMC, it is not a natural result of the RISM-polaron model.

A partial test of the validity of either model can be obtained from a direct comparison of the predicted positron annihilation rate with the experimental measurements. The thermally averaged positron decay rate can be evaluated from the Miller-Fan expression [18]

$$\langle\lambda\rangle=\rho\int d\mathbf{r}\, f(r)g(r)\ , \tag{19}$$

where $f(r)$ is the electron density of an atom fixed at the origin. Following Worrell and Miller [1], we take $f(r)$ as the electron distribution of the isolated xenon atom, determined here by the Laplacian of the first two terms of the potential (7) arising from tabulated Hartree-Fock wave functions for xenon. The decay rates for various fluid densities are given in Fig. 4 for the RISM-polaron theory and the PIMC calculation. As expected, since the RISM-polaron theory seems to underestimate the compression of the positron polymer and the density of xenon clusters surrounding the positron, the overall magnitude of the decay rate predicted by RISM-polaron theory is smaller than its PIMC partner. However, the shape of the curve is reproduced closely. We notice that the decay rate from the RISM-polaron calculation is not a monotonic curve in the region $\rho^*=0.4$–0.6. The apparent dip cannot be confirmed by either PIMC [1] or the experimental data [19], since they are only determined at a few densities. It is interesting that DFT calculations [19] show a similar local minimum in decay rate at 300 K, but it is located at a much lower fluid density.

IV. DISCUSSION AND CONCLUSIONS

As we mentioned above, PIMC is a numerically exact but time-consuming method, and it is all but impossible to use it to cover the complete range of the parameters needed for describing the system. On the other hand, since its predictions are qualitatively similar to those of PIMC calculations, the RISM-polaron theory has demonstrated its ability to describe positron localization in xenon. It has the advantage of allowing computations which cover a much larger range of parameters using present hardware. As demonstrated above, the RISM-polaron theory reveals the behavior of a thermalized positron at high fluid density, where the convergence of the PIMC simulations is extremely slow.

The behavior of the positron in xenon [1] is quite similar to that of an excess electron [3] because they share the same long-range attractive particle-solvent interaction. We have also applied the method presented here to an excess electron in xenon [20], employing the same electron-xenon potential that Coker, Berne, and Thirumalai used in their path-integral Monte Carlo studies [3]. We found that the predictions from the RISM-polaron theory are good, particularly for the electron-xenon pair distribution at high fluid densities [20]. Thus our results at high densities reported in this paper can be considered as a good

supplement to the PIMC calculations made only for fluid densities $\rho^*=0.01$, 0.05, 0.15, and 0.5 at $T=340$ K [1].

The interaction potential (7) is a smooth function with a strong repulsive core and an attractive tail, and it would be interesting to see the roles played in positron localization by each of the two components taken separately. Here, for the sake of comparison, we ignored the attractive polarization component and repeated the calculations as we did for the complete potential. As above, we obtained the corresponding P and $g(r)$, which have been plotted in Figs. 2 and 5, respectively. From Fig. 2 we see that removal of the attractive tail leads to a shift of the most compressed state of the positron polymer to a much higher density, accompanied by an increase in the amount of compression. Figure 5 clearly shows that $g(r)$ undergoes significant changes. For example, the xenon cluster formation has disappeared. It seems apparent that the repulsive potential is responsible for the compression of the positron polymer, and the attractive part for the fluid atom clustering. We can also see that $g(r)$ at $\rho^*=0.80$ in Figs. 3 and 5 are almost identical, which implies that $g(r)$ becomes less sensitive to the attractive potential when the fluid density is increased well above its critical value. This is not the case for the compression of the positron polymer (see Fig. 2). Since the positron decay rate λ largely depends on $g(r)$, its behavior reflects the nature of the attractive potential. In contrast, the momentum of the positron is largely related to the positron polymer compression [21], which depends on the repulsive potential. Even if the attractive part changes its dependence on the fluid density, we expect that the angular correlation of the annihilation photons, which depends on the momentum distribution of the positron, strongly reflects the nature of the repulsive potential.

We have seen that the RISM-polaron theory poorly reproduces PIMC results at low solvent density, and thus fails to correctly predict the behavior of localization of light particles on density fluctuations as revealed by PIMC calculations [1,3,22]. Chandler, Singh, and Richardson pointed out the problem in their first RISM-polaron paper and attributed it to the polaron approximation, which ignores large amplitude fluctuations [6(a)]. It would be interesting to explore a better approximation, but what we consider here is that the type of closure may also be an important issue. In practice, the functional $F[h(r)]$ in (2) must be approximated. The selection of a closure which is best for RISM-polaron theory and for a specific system needs to be justified, and is an independent problem in the theory of light particle localization. To explore the effect of varying the closure, we also tried the PY closure

$$c(r)=\{\exp[-\beta V(r)]-1\}[1+h(r)-c(r)]\ , \tag{20}$$

but we failed to achieve convergence for the given potential (7). The reason is far from clear to us. We also tried a closure analogous to Alnatt's modification of the PY closure [23], in which the short- and long-range parts of $c(r)$ and $v(r)$ are treated in a similar manner to our treatment of HNC closure presented in Sec. II.

$$c_s(r)=\exp[-\beta V_s(r)+\langle c_l\rangle][1+\theta(r)] -\langle c_l\rangle-\theta(r)-1\ . \tag{21}$$

This is just a linear version of the HNC closure (8) if $\theta(r)$ is small. However, the linearization leads to dependence on the manner in which the potential (7) is decomposed into short- and long-range components, whereas the HNC closure (8) allows arbitrary decomposition; whatever decomposition is convenient generates the same result. We tried two methods for decomposing the potential (7) for the PY closure (21). One is identical in form to that given earlier with the HNC closure, and the other is

$$V_l(r)=\begin{cases}-\alpha\{1-\exp[-(r/r_0)^6]\}/2r^4, & r>r_m\\ -\alpha\{1-\exp[-(r_m/r_0)^6]\}/2r_m^4, & r<r_m\ ,\end{cases}$$
$$V_s(r)=V(r)-V_l(r)\ , \tag{22}$$

where r_m is the place at which the polarization term in potential (7) attains its minimum value. We do get convergence for the closure with each choice of decomposition, but the results are very far from the Monte Carlo calculations. For example, there is no strong peak in $g(r)$. Although a better choice of decomposition may exist, so far we have not recognized the possibility of getting better results from the PY closure (21). A final remark regarding decomposition of the potential into short- and long-range components is that each selection effectively redefines the PY closure. The HNC closure seems the best closure available for our system at present.

It is worth pointing out that, so far, only the two-body polarization of xenon atoms has been considered in constructing the particle-solvent interaction for a positron in xenon. The interaction would be different if the many-body polarization effects were included. Many-body polarization has been shown to be extremely important in describing the behavior of an excess electron in fluid xenon [22,24]. It would be interesting to examine their effect on positron annihilation as well. We are consider-

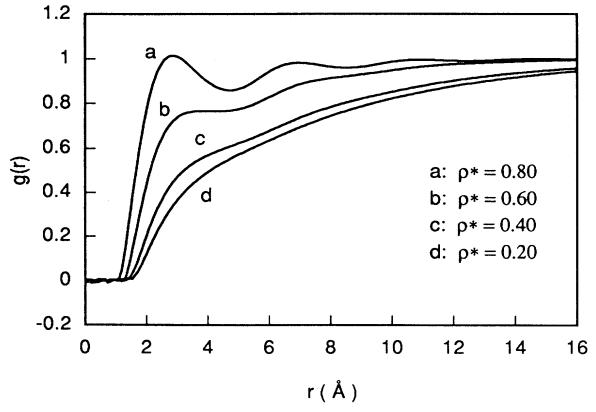

FIG. 5. The plot of $g(r)$ for various fluid densities at $T=340$ K from a RISM-polaron calculation using only the repulsive potential [the first term in (7)].

ing this problem for future work.

In summary, RISM-polaron theory provides a good foundation for the description of positron localization and annihilation in xenon. It has improved our understanding of the positron's behavior and its dependence on the positron-xenon interaction. But, in practice, one must be cautious in interpreting the quantitative predictions because the theory underestimates the strength of positron localization in xenon and therefore could benefit from some improvements.

ACKNOWLEDGMENTS

One of the authors (J.C.) benefitted from communications with F. Lado and we are grateful to him for allowing us to use his computer program for RHNC solutions. We also benefitted from conversations with T. Reese and Y. Fan. The support of the Robert A. Welch Foundation of Houston, Texas, through Grant No. P-1002 and the Research Foundation of Texas Christian University are greatly appreciated.

[1] G. A. Worrell and Bruce N. Miller, Phys. Rev. A **46**, 3380 (1992).
[2] Terrence Reese and Bruce N. Miller, Phys. Rev. E **47**, 2581 (1993).
[3] D. F. Coker, B. J. Berne, and D. Thirumalai, J. Chem. Phys. **86**, 5689 (1987).
[4] D. Chandler, in *Studies in Statistical Mechanics VIII,* edited by E. W. Montroll and L. J. Lebowitz (North-Holland, Amsterdam, 1982), p. 275, and references cited therein.
[5] (a) R. P. Feynman and A. R. Hibbs, *Quantum Mechanics and Path Integrals* (McGraw-Hill, New York, 1965); (b) R. P. Feynman, *Statistical Mechanics* (Benjamin, Reading, MA, 1972).
[6] (a) D. Chandler, Y. Singh, and D. M. Richardson, J. Chem. Phys. **81**, 1075 (1984); (b) A. L. Nichols, D. Chandler, Y. Singh, and D. M. Richardson, *ibid.* **81**, 5109 (1984); (c) D. Laria and D. Chandler, *ibid.* **87**, 4088 (1987).
[7] J. K. Percus and G. J. Yevick, Bull. Am. Phys. Soc. **5**, 275 (1960).
[8] G. Malescio and M. Parrinello, Phys. Rev. A **35**, 897 (1987).
[9] Fumion Hirata and Peter J. Rossky, Chem. Phys. Lett. **83**, 329 (1981).
[10] D. Laria, D. Wu, and D. Chandler, J. Chem. Phys. **95**, 4444 (1991).
[11] See, for example, M. J. Stott and E. Zaremba, Phys. Rev. Lett. **38**, 1493 (1977).
[12] D. Schrader, Phys. Rev. A **20**, 918 (1987); H. Nakanishi and D. Schrader, *ibid.* **34**, 1810 (1986).
[13] Yizhong Fan and Bruce N. Miller, J. Chem. Phys. **93**, 4322 (1990).
[14] C. Ng, J. Chem. Phys. **61**, 2680 (1974).
[15] F. Lado, S. M. Foiles, and N. W. Ashcroft, Phys. Rev. A **28**, 2374 (1983).
[16] Enrique Lomba, Mol. Phys. **68**, 87 (1989).
[17] Daniel Laria and David Chandler, J. Chem. Phys. **87**, 4088 (1987).
[18] Bruce N. Miller and Yizhong Fan, Phys. Rev. A **42**, 2228 (1990).
[19] (a) M. Tuomissaari and K. Rytsola, in *Positron Annihilation Studies of Fluids,* edited by S. Sharma (World Scientific, Singapore, 1988), p. 81; (b) M. Tuomissaari, K. Rytsola, and P. Hautojarvi, *ibid.*, p. 444.
[20] Jiqiang Chen and Bruce N. Miller (unpublished).
[21] Jiqiang Chen and Bruce N. Miller (unpublished).
[22] B. Space, D. F. Coker, Z. H. Liu, B. J. Berne, and G. Martyna, J. Chem. Phys. **97**, 2002 (1992).
[23] A. R. Allnatt, Mol. Phys. **8**, 533 (1964).
[24] Glenn J. Martyna and Bruce J. Berne, J. Chem. Phys. **90**, 3744 (1989).